A multi-technique analysis of gelatin biodegradation on core-shell nanoparticles surface by Alteromonas macleodii extracellular proteases

Sergio Fernández-Castillo Suárez, Cecile Courreges, Javier Jiménez-Lamana, Simon Godin, Sophie Nolivos, Regis. Grimaud, Luisa Ronga, Joanna Szpunar, Joachim Allouche

View Article Online
View Journal

Environmental Science Nano

Accepted Manuscript

This article can be cited before page numbers have been issued, to do this please use: S. Fernández-Castillo Suárez, C. COURREGES, J. Jiménez-Lamana, S. Godin, S. Nolivos, R. Grimaud, L. Ronga, J. Szpunar and J. Allouche, *Environ. Sci.: Nano*, 2023, DOI: 10.1039/D3EN00523B.

View Article Online
DOI: 10.1039/D3EN00523B

ARTICLE

A multi-technique analysis of gelatin biodegradation on core-shell nanoparticles surface by *Alteromonas macleodii* extracellular proteases

Received 00th January 20xx,
Accepted 00th January 20xx

DOI: 10.1039/x0xx00000x

Sergio Fernández-Castillo Suárez[a], Cécile Courrèges[a], Javier Jiménez-Lamana[a], Simon Godin[a], Sophie Nolivos[a], Régis Grimaud[a], Luisa Ronga[a], Joanna Szpunar[a] and Joachim Allouche[a*]

The study of interaction mechanisms at nanoscale between nanomaterials and microbial cells is of great importance in a wide range of research fields from health to environment. In the latter case, due to the high occurrence of nanoparticulate systems in the environment, the in-depth investigation of nanoparticles/bacteria interactions at nanoscale is needed to better understand the full picture of natural, chemical and biological processes of the microbial biodegradation of natural or manufactured organic nanoparticles in ecosystems. In this paper, we highlight for the first time the proof of the biodegradation process of gelatin adsorbed on nanoparticles surface by *Alteromonas macleodii* extracellular proteases. Using model core-shell gold@silica@gelatin nanoparticles, the biodegradation process has been demonstrated through a novel combined multi-technique approach using mass spectrometry (ToF-SIMS, LC-ESI-MS/MS, SP-ICP-MS), photo-electron spectroscopy (XPS) and electron microscopy (SEM, TEM).

Environmental significance

The mechanisms of interactions between nanomaterials and microbes in ecosystems is of major importance due mainly to the high bioavailability of nanoparticulated organic matter and the ongrowing dissemination of manufactured nanoparticles and nanoplastics in environment. Such interactions occuring at the nanoscale level remain poorly understood and have to be studied in-depth to better apprehend many complex processes like contaminant bioremediation or elemental biodegradation. We describe in the present work a direct proof of protein biodegradation by extracellular bacterial proteases occuring at the surface of model core-shell nanoparticles. We used a novel multi-technique analysis involving mass spectrometry and photo-electron spectroscopy characterizations allowing the identification of nanoscaled processes both in the incubation medium and on the particles surface.

1. Introduction

With the rise of Nanoscience during the last decades, the study, the design, the characterization and the applications of natural or manufactured nanomaterials have been the subject of many investigations in a wide range of industrial and research areas due to the exciting properties offered by nano-scaled dimensions[1–3]. But it is now well known that nanomaterials may strongly impact living systems by interacting with cells[4–6] and eventually crossing biological barriers[7,8]. Such interaction can be seen as two sides of a same coin as they may offer promising solutions in Nanomedicine[9] but may also induce moderate or adverse physiological responses[10,11] that have to be anticipated. In the field of environment, natural and manufactured organic or inorganic nanoparticles impair ecosystems functions where microorganisms at the bottom of the trophic chain drive important processes[12]. The study of the interactions between nanomaterials and microbes has to be carried out in depth to better understand and apprehend the full picture of many complex processes like the bioremediation of emerging contaminants[13–15] and/or the elemental cycles of natural biodegradation[16]. Studies dedicated to the characterization of bacteria/nanoparticles interactions are often carried out in the frame of the toxicity of nanoparticles[6] or the use of nanoparticles as killing agents for pathogenic bacteria[17]. Nevertheless, interaction of bacterial cells with nano-scaled objects is not restricted to nanoparticle toxicity but rather encompasses a large number of processes. For instance, in the ocean, bacteria access and degrade particulate organic carbon

[a] *Universite de Pau et des Pays de l'Adour, E2S UPPA, CNRS, Institut des Sciences Analytiques et Physico-chimie pour l'environnement et les matériaux (IPREM), UMR 5254, 2, avenue du président Angot, 64000 Pau, France.*

† Footnotes relating to the title and/or authors should appear here.
Electronic Supplementary Information (ESI) available: [details of any supplementary information available should be included here]. See DOI: 10.1039/x0xx00000x

that is, in part, present as particles with size in the nanometer range[18]. Nanoparticles can accelerate or inhibit the microbial degradation process of toxic and hazardous chemical compounds[19]. Micro- or nanoplastic particles can affect carbon cycle and carbon conversion by influencing microbial processes like CO_2 fixation, enzymes and genes expression[20,21]. Finally, bacteria/nanoparticles interactions are also of interest in nanoparticles bacterial biosynthesis[22].

However, the fundamental question related to the molecular mechanisms of organic compounds biodegradation by microbes at the nanoscale level is poorly studied. It is worth noting that such question is of major importance in environmental areas due to (i) the higher bioavailability of nanoparticulated organic matter compared to that of larger particles in environmental ecosystems and (ii) the dissemination of manufactured nanomaterials or nanoplastics that may affect or interfere with the natural biodegradation processes[18,20,21,23]. Indeed, it is well known that the surface properties of nanoparticles trigger their ability to bind and vectorize small or macromolecular organic entities including organic substrates through electrostatic, covalent or coordination binding[24,25]. However, the accessibility of extracellular bacteria enzymes to substrates attached or deposited on the surface of nanoparticles and their subsequent degradation at nanoscale has never been directly demonstrated to date. Indeed, such direct demonstration requires a non-trivial implementation of a panel of characterization techniques able to return molecular and elemental information both from surface and bulk at the nanoscale level.

In this paper, we provide, for the first time, direct evidences of a nanoscale biodegradation process of substrate adsorbed on the surface of model core-shell nanoparticles by *Alteromonas macleodii* ATCC 27126 extracellular enzymes. *Alteromonas macleodii* are aerobic gram-negative marine bacteria known to produce a variety of enzymes, including gelatinase, amylase or lipase[26–28]. These bacteria exhibit a fast growth and an opportunistic copiotrophic behavior in both cold and warm water oceans[26,28–30]. They are known to play important roles in the regulation of the iron and carbon cycles[31–34] and to grow with organic matter in particulate form[35] as well as being adapted to degrade algal polysaccharides[32].

The mechanism of surface biodegradation has been evidenced through a multi-technique characterization approach relied on the analyses of both nanoparticles and incubation supernatant containing bacterial proteases. Single Particle Inductively coupled plasma mass spectrometry (SP-ICPMS), liquid Chromatography Electrospray Ionization Tandem Mass Spectrometry (LC-ESI-MS/MS), Time-of-Flight Secondary Ion Mass Spectrometry (ToF-SIMS), X-Ray photoelectron spectroscopy (XPS) and Electron Microscopy (SEM and TEM) have been implemented to provide and combine complementary information. The hierarchical architecture of the model nanoparticles featuring a core-shell gold@silica@gelatin (Au@Si@Gel) morphology has been specifically designed in order to control their physico-chemical properties as well as the level of surface area of contact between nanoparticles and bacteria proteases.

2. Experimental

All chemicals and reactants for synthesis of nanoparticles, bacteria growth and incubation experiment were supplied by Sigma (ACS Grade) and used without further purification.

2.1 Gold@silica@gelatin nanoparticles synthesis.

The synthesis of the core-shell nanoparticles had three different steps: gold core synthesis, silica shell addition and gelatin layer coating.

First gold nanoparticles (AuNPs) of 30 ± 6 nm in diameter were synthetized following the Turkevich method[36] 2.8 mL of a 0.25 g/100 ml of $HAuCl_4$ solution were added to 47.2 mL of Milli-Q water and heated to a temperature of 98 °C. Then, 0.75 mL of a 38.8 mM solution of trisodium citrate $Na_3C_6H_5O_7$ were quickly added. After 5 min stirring, the reddish particles solution was finally removed from heat source and left stirring until complete cooling to room temperature.

The silica shell was subsequently coated on the gold core by a sol-gel synthesis[37]. Typically, 8 mL of the as prepared AuNPs solution were diluted in 40 mL of isopropanol. Under stirring, 1 mL of ammonium hydroxide concentrated solution (NH_4OH 30%) was injected. After 2 min stirring, 100 µL of tetraethyl orthosilicate TEOS were added. The recipient was closed and the reaction was left to occur overnight leading to gold@silica particles (Au@Si).

The final particles were centrifuged and washed three times and concentrated to a volume of 15 mL of Milli-Q water. Meanwhile, a gelatin solution was prepared dissolving 50 mg of type A gelatin from porcine skin (bloom 300) in 10 mL of Milli-Q water. Both solutions were stirred and heated to 40 °C, and after the nanoparticles were added on the gelatin. The gold@silica@gelatin nanoparticles (Au@Si@Gel) were centrifuged and washed 4 times and finally stored at 4 °C.

2.2 Bacteria culture and growth conditions.

The strain used in this study was *Alteromonas macleodii* ATCC 27126. The bacteria were routinely maintained on SSW agar plates medium at 30 °C. Synthetic seawater (SSW) was prepared (NaCl 0.2 mol·L^{-1}, KCl 10 mmol·L^{-1}, Tris-HCl 50 mmol·L^{-1} pH 7.8, NH_4Cl 56 mmol·L^{-1}, K_2HPO_4 427 µmol·L^{-1}, $FeSO_4$ 8 µmol·L^{-1}, $MgSO_4$ 65 mmol·L^{-1} and $CaCl_2$ 13 mmol·L^{-1}) using a solution of sodium acetate 20 mmol·L^{-1} as a carbon source. The liquid cultures were incubated at 30 °C under shaking at 250 rpm.

2.3 Proteolytic activity test.

Proteolytic colorimetric assays[38,39] were performed in Tris 25 mM pH 7.5, azocasein 5 mg/mL, in a final volume of 0.5 mL. Mixtures were preincubated at 30 °C for 1 hour and the reaction started by addition of Proteinase K at 0.5 µg/mL or 250 µL of culture supernatant at OD = 0.5, which is equivalent to 5×10^8 cells/mL. After 30 min of incubation the reaction was stopped by precipitating of the protein by TCA addition and centrifugation for 20 min, 10000 rpm at 4 °C. The acid soluble peptides generated by digestion of azocasein were detected in the supernatant by measuring the absorbance at λ = 440 nm. A

View Article Online
DOI: 10.1039/D3EN00525B

replicate measurement of a positive control using Proteinase K (PK) give an average optical density (OD) value that is considered as having 100% proteolytic activity. In consequence, the average of 3 biological replicates and 3 technical replicates of the extracellular enzymes from A. macleodii cultured with sodium acetate give an OD value corresponding a percentage of the proteolytic activity of the PK. The negative control replicate of the culture medium containing no enzymes give 0 % proteolytic activity.

2.4 Incubation experiment.

In order to track peptides coming from the degradation process, bacteria cells have to be removed from the incubation medium containing extracellular proteases in order to avoid peptides metabolization by bacteria or artefact that may come from the detection of intracellular peptides.

To perform the incubation experiment (Fig. 1), 1 mL of the SSW liquid *A. macleodii* overnight culture was taken and centrifuged at 13200 rpm. The culture medium was therefore separated from the bacteria pellet. In parallel, 500 µL of Au@Si@Gel nanoparticles were centrifuged at 13200 rpm. The pellet of nanoparticles was thoroughly redispersed in 100 µL of the previously stated protease-containing culture medium.

The incubations were performed in a water bath at 30 °C. One sample of Au@Si@Gel was incubated for 30 min and the other for 60 min. In addition to these samples, two control samples were prepared: the culture medium after bacteria removal by centrifugation incubated 60 min and a control of Au@Si@Gel nanoparticles incubated in medium without bacteria for 60 min. After the incubation was completed, each sample was removed from the bath and centrifuged at 13200 rpm to separate them into two subsets of samples, adding to a total of seven: pellet of control Au@Si@Gel incubated 60 min without proteases, pellet of Au@Si@Gel incubated 30 min, pellet of Au@Si@Gel incubated 60 min, supernatant of control Au@Si@Gel incubated 60 min without proteases, supernatant of Au@Si@Gel incubated 30 min, supernatant of Au@Si@Gel incubated 60 min and culture medium separated from bacteria (plus the Au@Si and Au@Si@Gel that were not incubated).

On one hand, the supernatants were recovered and stored inside a freezer at -20 °C before their analysis by LC-ESI-MS. On the other hand, the pellets of nanoparticles were redispersed in a small volume of milli-Q water, and were also stored at -20 °C before preparation for ToF-SIMS and XPS analyses.

2.5 Characterization

2.5.1 Scanning Electron Microscopy (SEM)

The SEM images were obtained using a JEOL JAMP 9500F Auger Microprobe spectrometer (JEOL Ltd., Tokyo, Japan) working under UHV conditions (pressure < 2.10^{-7} Pa). A drop of the sample was deposited on aluminum foil and dried in the oven before analysis. The analyses were performed at current and tension values of 5 nA and 30 keV respectively.

2.5.2 Transmission Electron Microscopy (TEM) images of the nanoparticles.

TEM images of the AuNPs, Au@Si and Au@Si@Gel were captured by a Philips CM 200 (200 kV) instrument equipped with a LaB6 source. A drop of the sample was deposited on a carbon coated copper grid and dried at room temperature before analysis.

2.5.3 Single-Particle Inductively Coupled Plasma Mass Spectrometry (SP-ICP-MS) analyses of the nanoparticles.

Nanoparticles were size characterized and quantified by a NexION 5000 multi quadrupole ICP Mass Spectrometer with a Syngistix Nano Application Module (PerkinElmer, Shelton, CT, US). This technique allows to analyze individual nanoparticles and provides information on both particle size and concentration for very dilute nanoparticle suspensions. Briefly, the intensity of the signal (Au or Si) per NP registered by SP-ICP-MS is transformed into mass of the element per NP. In addition, in the case of solid spheres of known density, the mass of the element per NP can be transformed into size. While this calculation is valid for the Au core of the Au@Si@Gel nanoparticles, this is not the case for the SiO_2 shell. Instead, an equivalent diameter can be calculated, i.e. the size of a theoretical solid nanoparticle composed of pure SiO_2

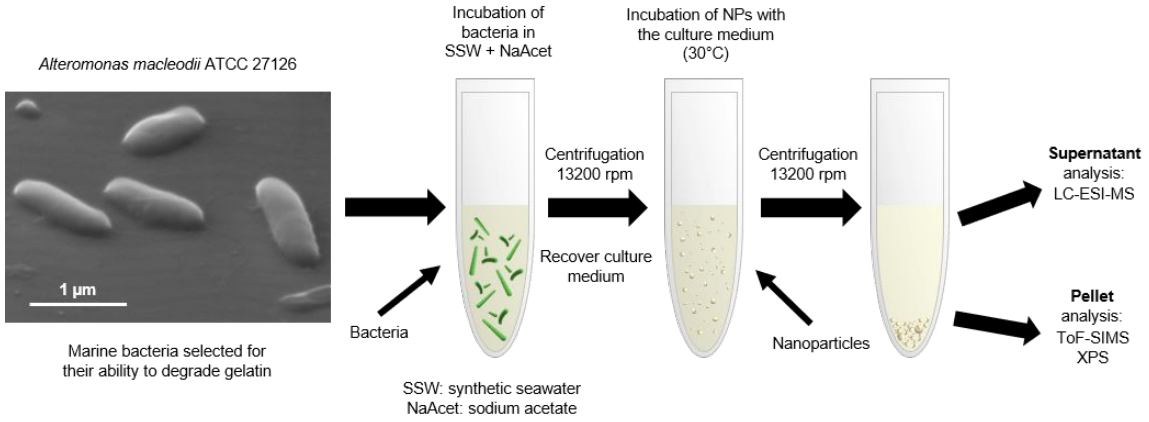

Fig. 1. Scheme of the experimental protocol for the study of the gelatin biodegradation at the surface of nanoparticles by *A. macleodii* proteases.

View Article Online
DOI: 10.1039/D3EN00523B

corresponding to the calculated mass. Suspensions were diluted in ultrapure water prior the SP-ICP-MS analysis in order to have around 3000 particles detected in each run. Au and Si signals were monitored with a dwell time of 100 µs and a total acquisition time of 100 s. In the case of the Au signal, the m/z at 197 was monitored using only the third quadrupole, Q3.

As for the Si signal, the instrument operated in "mass-shift" mode in order to remove the interferences at the m/z 28 and by using O_2 as reaction cell gas, which allows the analysis of ^{28}Si by monitoring the oxide ion at m/z ± 16 u. Therefore, the first quadrupole was set to m/z 28 (the precursor ^{28}Si ion) and the third quadrupole was set to m/z 44 (the target product ion $^{28}Si^{16}O$). Transport efficiency was calculated daily by using a standard suspension of AuNPs with a nominal diameter of 32.7 ± 2 nm (LGC, Teddington, UK). Particle size distributions were obtained by MagicPlot from raw data provided by the module.

2.5.4 Time-of-Flight Secondary Ion Mass Spectrometry (ToF-SIMS) analyses.

ToF-SIMS analyses of the pellets and supernatants were carried out using a TRIFT V NanoToF II Tandem MS (Physical Electronics, Chanhassen, MN, US) instrument equipped with a 30 kV Bi_n^{q+} LMIG primary ion gun. Samples were prepared by adding drops on aluminum foil and letting them dry, assuring a flat surface.

The mass spectra were acquired in both positive and negative polarities at room temperature and using the same analytical conditions to ensure a semi-quantitative analysis.

The LMIG gun was tuned to release Bi_3^{++} clusters primary ions over 50 × 50 µm raster size with a 3.28×10^{12} ion/cm^2 ion dose, for 30 frames for surface analyses. For Tandem MS analyses, the selected precursor ion was sent into the CID activation cell and analyzed in MS^2. Charge compensation was used for all analyses.

Data processing was performed using ToF-DR software supplied by Physical Electronics. All negative polarity mass spectra were calibrated using OH^- (m/z 17.00), C_2H^- (m/z 25.00) and Cl^- (m/z 34.97) peaks while all positive polarity mass spectra were calibrated using Na^+ (m/z 22.99), $C_2H_2^+$ (m/z 26.01) and $C_2H_3^+$ (m/z 27.02).

2.5.5 Liquid Chromatography Electrospray Ionization Tandem Mass Spectrometry (LC-ESI-MS/MS) analyses.

Chromatographic separations were performed on a C18, 1 × 150 mm, 5 µm, 300 Å column, with mobile phase A (H_2O, 0.1% formic acid) and B (acetonitrile, 0.1% formic acid).

Detection was ensured by an Orbitrap Fusion Lumos High Resolution Mass Spectrometer (Thermo Fisher Scientific, Waltham, MA, US) with Full MS scans performed at R = 120000 every 1.5 s and MS^2 scans in between (at R=30000, precursors were filtered for signals showing a peptide-like isotopic pattern).

The samples were an instrumental blank, the incubation medium after removing the bacteria, a Au@Si@Gel control incubated for 60 minutes in culture medium without bacteria, a positive control of trypsin-digested gelatin and two samples of Au@Si@Gel incubated with the bacteria medium at 30 and 60 min. All samples were filtered through 10 kDa cut-off filter after a 2-fold dilution with water, and then diluted another 5-fold with 90:10 H_2O:ACN 0.1% formic acid before injection.

Data processing was performed employing DeNovoGUI, an open-source software provided by CompOmics[40], selecting oxidation of methionine and oxidation of proline as variable chemical modifications, 10 ppm precursor mass tolerance and 5 ppm fragment mass tolerance. Through this software it was possible to analyze the MS^2 spectra and *de novo* sequencing a series of peptides present in the samples, allowing to compile lists of peptides found in the positive control and the samples incubated 30 and 60 min. The corresponding proteins were later identified using the Basic Local Alignment Search Tool (BLAST) tool on UniProt[41]. Furthermore, when DeNovoGUI provided with gapped sequences they were further analyzed with ProSight Lite to confirm the identity of the assigned amino acids and the validity of the complete sequences[42]. Knowing the identities of the proteins present in the control and samples and the lists of *de novo* sequenced peptides it was possible to calculate the protein coverage of said proteins.

2.5.6 X-ray Photoelectron Spectroscopy (XPS) analyses.

XPS analyses of the pellets and supernatants were performed with a Thermo K-alpha Spectrometer (Thermo Fisher Scientific, Waltham, MA, US) with a hemispherical analyzer and a microfocused monochromatized radiation Al Kα line (1486.6 eV) operating at 75 W under a residual pressure of 1×10^{-7} mBar with 400 µm spot size. A pass energy of 20 eV was used for core peak records. A flood gun, which sprays low energy electrons and Ar^+ ions over the sample surface to minimize the surface charging, was used during the analysis for neutralization.

For the XPS spectra fitting and data processing the CasaXPS software was employed. The binding energies for all elements and components were calibrated referencing to the C 1s hydrocarbon peak at 285.0 eV. Core peaks were analyzed using a Shirley background and peak positions and areas were obtained by a weighted least-squares fitting of model curves (70% Gaussian, 30% Lorentzian) to our experimental data. Quantification of surface composition was based on Scofield's relative sensitivity factors.

3. Results

Hybrid core-shell gold@silica@gelatin nanoparticles (Au@Si@Gel) (Fig. 2a) with a hierarchical structure composed of a one single gold core, a silica shell and a gelatin outer layer have been synthesized through a sequential method. Such morphology was specifically designed to achieve a perfect control of the experimental conditions.

View Article Online
DOI: 10.1039/D3EN00533D

3.1 Synthesis of Au@Si@Gel nanoparticles

First, gold cores (AuNPs) with median diameter of 30 ± 6 nm statistically measured on 30 particles on TEM images were obtained (Fig. 2b) through a Turkevich method[36] but adapted to our case using citrate as stabilizing agent. The size obtained by TEM was in good agreement with the results obtained by SP-ICP-MS (Fig. 2f). This technique is element sensitive and allows to obtain the mass of the element measured per nanoparticle and, hence, by knowing the density and assuming that the particles are spherical, the size distribution of nanoparticles can be evaluated[43]. When monitoring the Au signal, a median diameter of 28 ± 2 nm related to the size of the Au core of the Au@Si@Gel nanoparticle was obtained (Fig. 2f). In addition, quantitative information such as the nanoparticle concentration of the original suspension was estimated to 3.3×10^{11} nanoparticles per mL by SP-ICP-MS. This concentration was used in the next step to control the number of particles added to the incubated samples with bacteria proteases.

The addition of a silica shell around the gold cores by a sol-gel reaction[37] was subsequently carried out using tetraethyl orthosilicate (TEOS) precursor as the silica source. Such method, inspired by a recent protocol developed by our group, has been carried out due to its ability to lead monodisperse silica nanoparticles and a good control of the silica shell thickness[44,45] evaluated to 64 ± 6 nm by TEM low and high magnification images in Fig. 2c and Fig. 2d respectively. The sizes of the Au@Si and Au@Si@Gel were measured to 158 ± 6 nm and 165 ± 10 nm by TEM on a set of 100 particles. The gelatin layer thickness of Au@Si@Gel was hence evaluated to less than 10 nm. Although SP-ICP-MS cannot provide information about the thickness of the nanoparticles shell, by considering the density and molar mass fraction of SiO_2, a median equivalent diameter of 132 ± 6 nm (see experimental section) was obtained for the Au@Si@Gel (Fig. 2g). This provides an evaluation of the whole core-shell Au@Si@Gel particle size of 160 ± 6 nm, which is in good agreement with the TEM images.

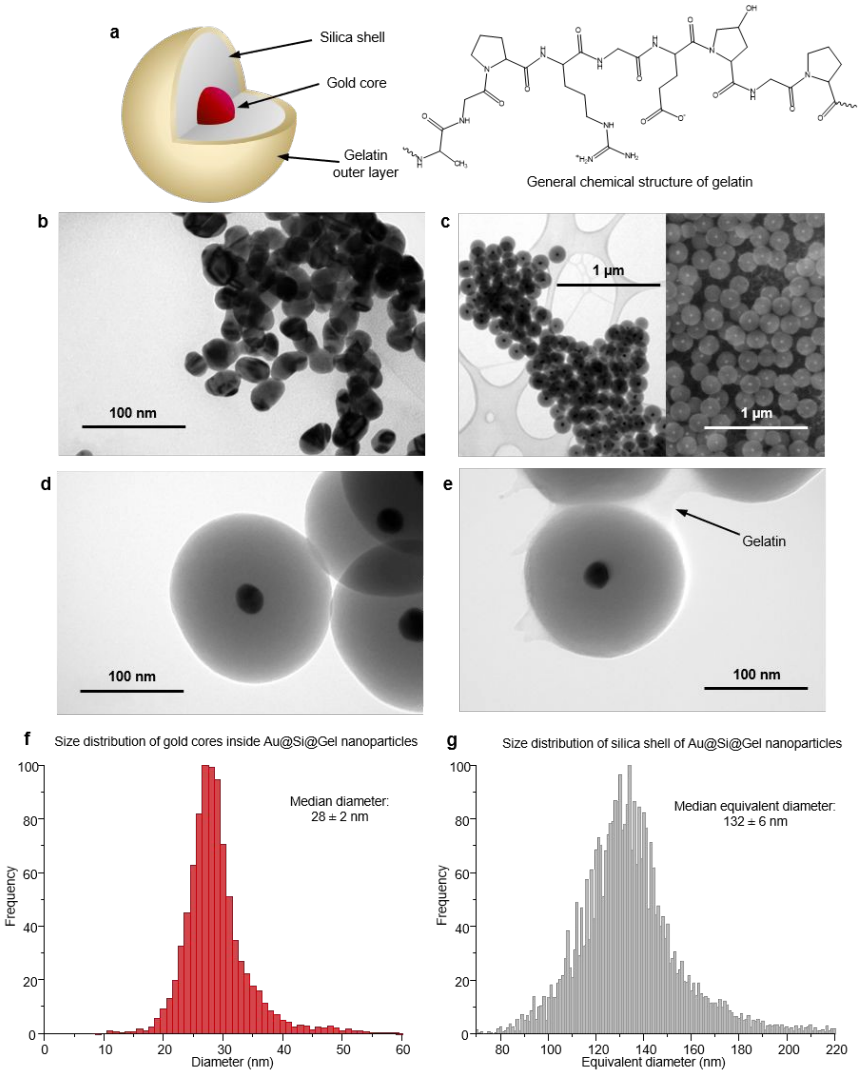

Fig. 2 Characterization of synthesized core-shell nanoparticles. a, Three-dimensional model of a gold@silica@gelatin nanoparticle (Au@Si@Gel) and general chemical structure of gelatin. b, TEM image of gold nanoparticles (AuNPs). c, TEM (left) and SEM (right) low magnification images of gold@silica nanoparticles (Au@Si). d, TEM high magnification image of Au@Si nanoparticles. e, TEM high magnification image of a Au@Si@Gel nanoparticle. f, Particle size distribution of the gold cores obtained by SP-ICP-MS. g, Particle size distribution of the silica shell obtained by SP-ICP-MS.

View Article Online
DOI: 10.1039/D3EN00523B

In addition, it is worth noting that the silica layer has a dual role for the study. Firstly, it allows to target the whole particles size by generating a silica shell on one single gold core with a controlled thickness. Indeed, the size dispersity of the particles has to be reduced in order to control the level of interface between substrate and proteases, and thus, generate a homogeneous surface of contact per particles. Secondly, the silica shell offers an accurate platform for the adsorption of the gelatin substrate layer through electrostatic interactions. Indeed, the pH value used in our experiments is 8 which leads to negatively charged nanoparticles due to the deprotonated silanol groups and, simultaneously, positively charged gelatin protein (isoelectric point close to 9.5). This leads to stable oppositely charged silica/gelatin complex already designed and characterized in previous works by our group[46,47].

ToF-SIMS (Fig. 3b). Concerning Au@Si@Gel nanoparticles, XPS O 1s, N 1s and C 1s core peaks exhibit chemical environments characteristic of gelatin similar to the ones of type A gelatin reference (Fig. 3a). Indeed, two components were detected on the O 1s core peak. The one at 531.36 eV is assigned to an oxygen in **O**=C-O and **O**=C-N environments (6.97 atomic percent concentration, At.%) and the main one at 532.67 eV is attributed to **O**-C=O and mainly **O**-Si environments (25.5 At.%). In the gelatin sample it is clear that **O**-C=O is a minority component compared to **O**=C-O and **O**=C-N. For the Au@Si, only a major **O**-Si environment is detected (57.82 At.%). The peptide bond environment can also be identified in the N 1s core peak of the Au@Si@Gel sample at a binding energy of 400.04 eV (11.03 At.%) as well as **N**=C-NH and **N**-C environments at 398.54 eV, less prevalent (0.46 At.%). N 1s

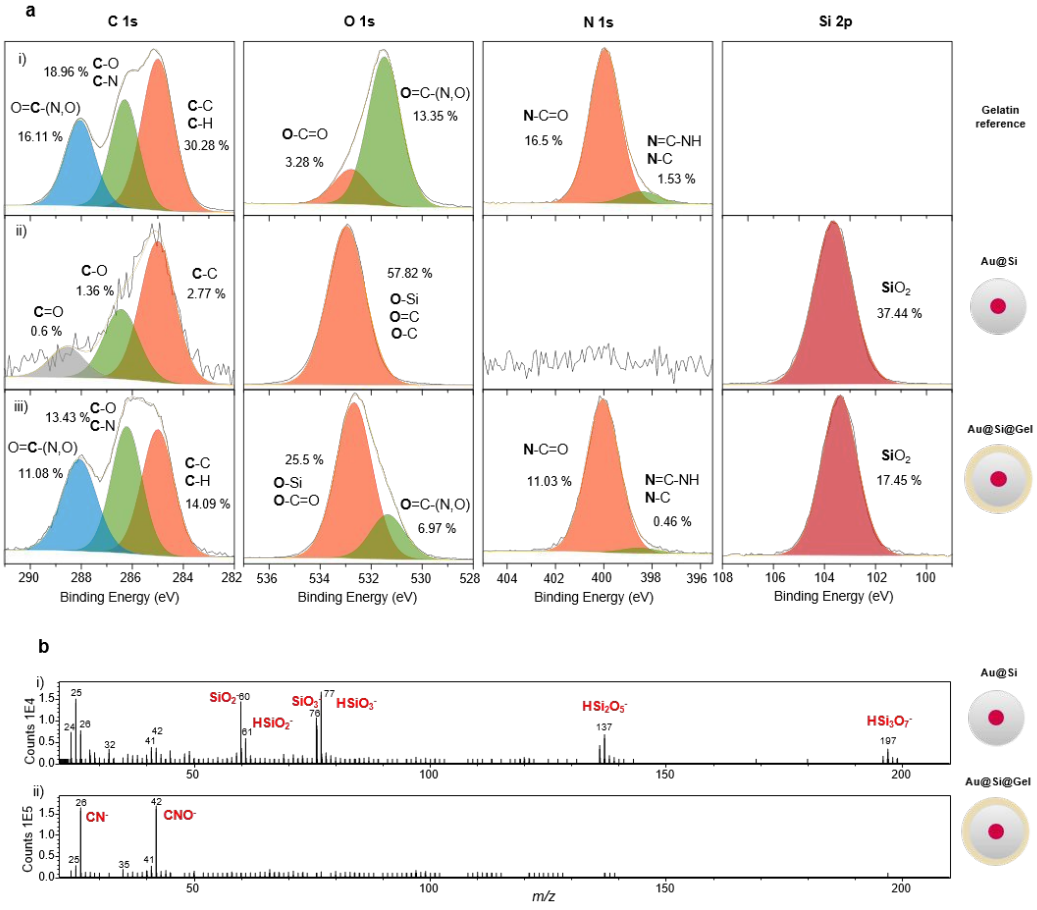

Fig. 3 XPS and ToF-SIMS characterization of core-shell nanoparticles before biodegradation. a, XPS C 1s, O 1s, N 1s and Si 2p core peaks spectra of i) gelatin reference, ii) Au@Si and iii) Au@Si@Gel; b, ToF-SIMS spectra in negative polarity of i) Au@Si and ii) Au@Si@Gel, over 20 to 210 m/z range; the characteristic peaks are labelled in red..

The gelatin outer layer is finally deposited on the gold@silica particles (Au@Si) using a gelatin solution at 37 °C. Purified Au@Si@Gel (Fig. 2e) exhibit a thin gelatin layer (<10 nm) visible on TEM images, which is not the case for Au@Si particles (Fig. 2d).

3.2 Surface characterization of Au@Si@Gel nanoparticles

To characterize the chemical composition of Au@Si and Au@Si@Gel nanoparticles surface before interaction with proteases, such particles were analyzed by XPS (Fig. 3a) and signal is not detected for Au@Si nanoparticles. Concerning the C 1s core peak, three components were found for Au@Si@Gel. The one at 285 eV is related to the aliphatic carbon of the gelatin and the adventitious carbon (14.09 At.%), the one at 286.22 eV refers to **C**-O/**C**-N environments from the gelatin molecule (13.43 At.%) and the one at 288.08 eV to the O=**C**-N environment (11.08 At.%). On the other hand, for the Au@Si, **C**-C (2.77 At.%), **C**-O (1.37 At.%) and **C**=O (0.6 At.%) are detected in lower concentrations (Table S1a, S1b and S1c ESI†).

View Article Online DOI: 10.1039/D2EN00527B

ToF-SIMS analyses were also performed on the samples to identify molecular species at the extreme surface of the nanoparticles before biodegradation. In the negative polarity, the mass spectrum of Au@Si nanoparticles displays a series of characteristic peaks of the silica shell such as SiO_2^- (m/z 59.97), $HSiO_2^-$ (m/z 60.97), SiO_3^- (m/z 75.96), $HSiO_3^-$ (m/z 76.96), $HSi_2O_5^-$ (m/z 136.93) and $HSi_3O_7^-$ (m/z 196.9). These peaks were either absent or had low intensity in the spectra of the intact Au@Si@Gel, where gelatin protein peaks CN^- (m/z 26.00) and CNO^- (m/z 42.00) were detected (Fig. 3b). In the positive polarity, a characteristic Si^+ peak (m/z 27.98) was observed for Au@Si but not for Au@Si@Gel, where only gelatin-related peaks, like CH_2N^+ (m/z 28.02) and CH_4N^+ (m/z 30.04) were detected (Fig. S1 ESI†).

3.3 Detection of protease activity in the culture medium of *A. macleodii* by a proteolytic assay.

To confirm the presence of extracellular enzymes produced by *A. macleodii* ATCC 27126 a colorimetric azocasein assay (Fig. 4) was performed to detect proteolytic activity was used[38,39]. Compared to the culture medium that did not contain enzymes and showed no activity, an optical density (OD) of 0.17 ± 0.2 was measured for the *A. macleodii* culture supernatant, indicating that the azocasein had been digested by enzymes produced by bacterial cells during growth with sodium acetate as a carbon source. This activity corresponds to 31.43 % of the activity obtained with 5 µg/mL of Proteinase K. Although the substrate in this assay was not gelatine, we confirmed that *A. macleodii* produces extracellular enzymes in our culture conditions. In order to study the ability of these extracellular proteases to access to the substrates attached on the surface of nanoparticles, the biodegradation experiments were performed with the culture supernatant in absence of bacteria to avoid any interference coming from the particles/cells

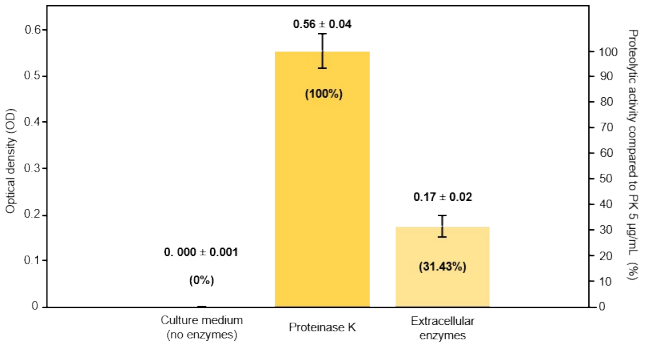

Fig. 4. Detection of proteolytic activity by extracellular enzymes produced by *A. macleodii.*

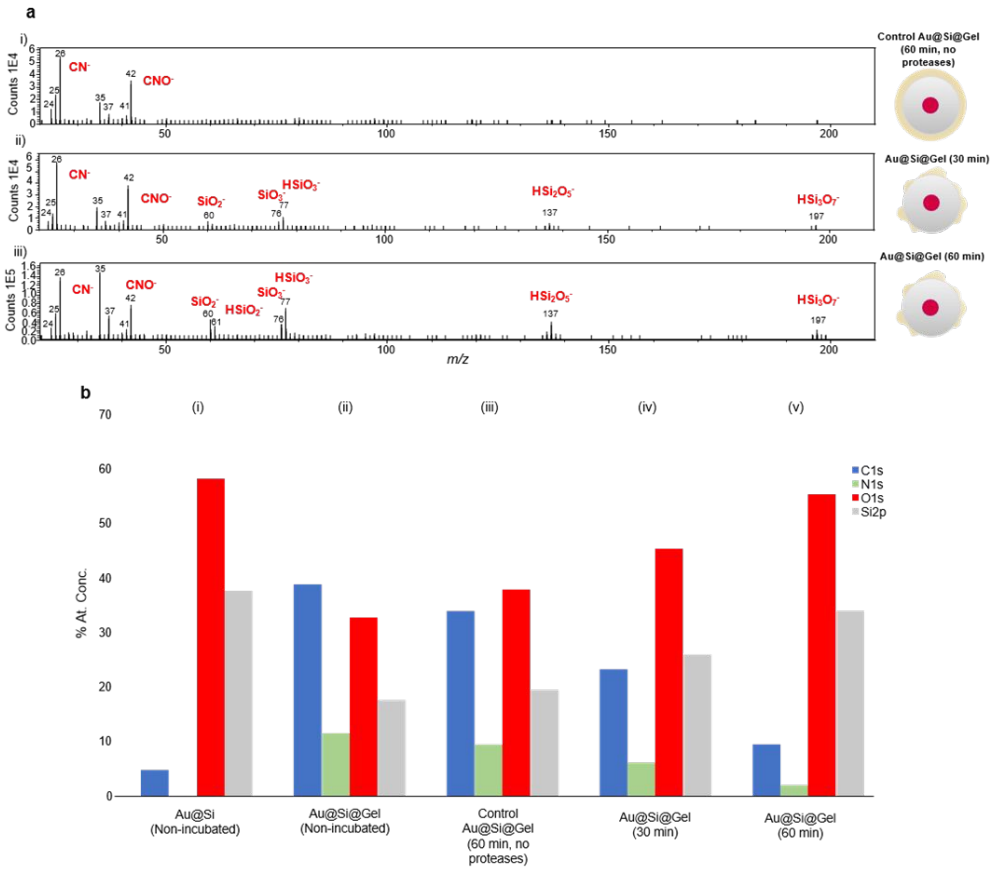

Fig. 5. ToF-SIMS and XPS analyses of surface of control particles and incubated particles with proteases. a, ToF-SIMS spectra in negative polarity of i) control Au@Si@Gel incubated 60 min without proteases, ii) Au@Si@Gel incubated 30 min and iii) Au@Si@Gel incubated 60 min over 20 to 210 m/z range; the characteristic peaks are labelled in red. b, Histogram representing the At.% of C 1s (blue), N 1s (green), O 1s (red) and Si 2p (grey) elements detected at the surface of i) non-incubated Au@Si, ii) non-incubated Au@Si@Gel, iii) control Au@Si@Gel incubated 60 min without proteases, iv) Au@Si@Gel incubated 30 min and v) Au@Si@Gel incubated 60 min, and calculated from the quantitative XPS analysis.

View Article Online
DOI: 10.1039/D3EN00527B

interactions. In addition, since one of the main objectives is to identify peptides coming exclusively from the gelatin degradation process, cells had to be removed from culture supernatant to prevent metabolization or artefacts coming from the detection of intracellular peptides.

3.4 XPS and ToF-SIMS analysis of nanoparticles surface after incubation with proteases.

ToF-SIMS was used to obtain extreme surface elemental and molecular information from the pellets of nanoparticles after interaction with extracellular proteases. In negative polarity for the Au@Si@Gel incubated 30 and 60 min in the culture medium the characteristic peaks from the silica shell SiO_2^- (m/z 59.97), $HSiO_2^-$ (m/z 60.97), SiO_3^- (m/z 75.96), $HSiO_3^-$ (m/z 76.96), $HSi_2O_5^-$ (m/z 136.93) and $HSi_3O_7^-$ (m/z 196.90), previously found in the Au@Si, were detected (Fig. 5a). These peaks where either absent or had low intensity in the spectra of the control Au@Si@Gel incubated 60 min without proteases. Protein-related peaks such as CN^- (m/z 26.00) and CNO^- (m/z 42.00) were detected in all samples. This comes as a proof of a partial degradation of the gelatin layer at the surface of the nanoparticles incubated with proteases. Furthermore, the intensity of the silica-related peaks was higher after 60 min of incubation than after 30 min, showcasing the influence of incubation time in the degradation process. Moreover, the confirmation of the assignment of these peaks was achieved thanks to a ToF-SIMS Tandem MS analysis, where the precursor ion $HSi_3O_7^-$ (m/z 196.90) was sent into a CID activation cell and the consecutive losses of SiO_2^- or $HSiO_2^-$, shown as -60 or -61 respectively, were observed (Fig. S2 ESI†). In the positive polarity, the characteristic Si^+ peak (m/z 27.98) was found for the incubated Au@Si@Gel samples at 30 and 60 min (Fig. S3 ESI†). This was not the case for the non-incubated nanoparticles and the control Au@Si@Gel incubated without proteases, where only gelatin-related peaks were detected like CH_2N^+ (m/z 28.02).

Additionally, XPS analyses revealed complementary information on the chemical composition of the samples surface. A comparison of the XPS spectra of the control Au@Si@Gel incubated without proteases, and the Au@Si@Gel incubated 30 and 60 min reveals the same components and environments for C 1s, O 1s, N 1s and Si 2p core peaks (Fig. S4 ESI†). Especially, the peptide bond environments characteristic of the gelatin can be identified in N1s and C1s spectra at 400 eV and 288 eV respectively. The detailed components and quantitative analysis are presented in Table S1 ESI†. By comparing the reference Au@Si@Gel and control 60 min incubated Au@Si@Gel without proteases (Fig. 5b), the elemental compositions are very similar. A slight difference can be noticed with a small reduction of carbon from 38.6 At.% to 33.77 At.% and nitrogen from 11.49 At.% to 9.32 At.% as well as a small increase of oxygen from 32.47 At.% to 37.61 At.% and silicon from 17.45 At.% to 19.29 At.% for reference Au@Si@Gel and control Au@Si@Gel respectively. In addition, the quantitative XPS analyses showed, by comparing to the control particles, a clear tendency of an increase in the atomic percent concentrations for both oxygen and silicon in the samples after 30 min and 60 min of incubation. Indeed, oxygen increases from 45.05 At.% to 57.97 At.% and silicon from 25.79 At.% to 33.71 At.% between 30 and 60 min (Fig. 5b). This can be attributed as an increasing exposure of the silica shell due to gelatin degradation with the incubation time in presence of extracellular proteases. Such gelatin degradation process is further reinforced by the strong decreases of carbon from 23.12 At.% and 9.39 At.% and nitrogen from 6.05 At.% to 1.93 At.% for Au@Si@Gel incubated with proteases for 30 min and 60 min respectively.

3.5 Detection and identification through LC-ESI-MS analysis of peptides release in supernatant after incubation.

LC-ESI-MS/MS was carried out to analyze the supernatants from the incubation mix of nanoparticles and culture medium to identify proteolytic peptides coming from the degradation of gelatin. This technique has already been used in studies related to gelatin identification and differentiation[48–52]. To assess the fraction of peptides coming from the degradation of gelatin with the incubation time, Au@Si@Gel nanoparticles incubated in absence of proteases were also analyzed, as well as the culture media after 30 min and 60 min of incubation. In addition, the culture medium after bacteria removal incubated 60 min and a positive control of trypsin-digested gelatin were also analyzed to make sure the possible peptides detected in the samples do not come from the culture medium, and to be able to identify the signal of the gelatin respectively. When comparing the resulting Total Ion Current (TIC) chromatograms, peaks specific from the samples can be detected between 2.5 min and 10 min of retention time, which is not the case for the controls (Fig. 6a). Focusing on the Extracted Ion Current (XIC) chromatograms of the samples incubated 30 and 60 min at m/z 842.41, m/z 890.43 and m/z 824.42, an increase in intensity with incubation time was detected in all three of them, which indicates a higher quantity of peptides had been released (Fig. 6a).

From the resulting MS/MS data, it was possible to *de novo* sequence a series of peptides, using DeNovoGUI[40]. Peptides, such as GVQGGKGEQGPAGP**P**GFQ (m/z 842.41), GA**P**GTAGPSGPSGLPGERGAA (m/z 890.43), and GLMGPRGP**P**GAVGA**P**GPQ (m/z 824.42), where the **P** indicates hydroxyproline, were successfully sequenced and identified (100% identity) in the UniProt database as part of the Collagen type I alpha 2 chain protein of *Sus scrofa*, with E-value 6.4E-13, 8.4E-15 and 7.3E-13 respectively (Fig. 6b)[41]. A complete list of the identified peptides can be consulted in the Table S2 ESI† for the positive gelatin control and in the Tables S3 and S4 ESI† for the supernatant of Au@Si@Gel incubated in the culture medium for 60 minutes and 30 minutes respectively. Some of these peptides were presented as gapped by DeNovoGUI. The gaps in the peptide sequences were completed by inference of the protein sequences. The amino acid assignment was confirmed with ProSight Lite[42].

View Article Online
DOI: 10.1039/D3EN00523B

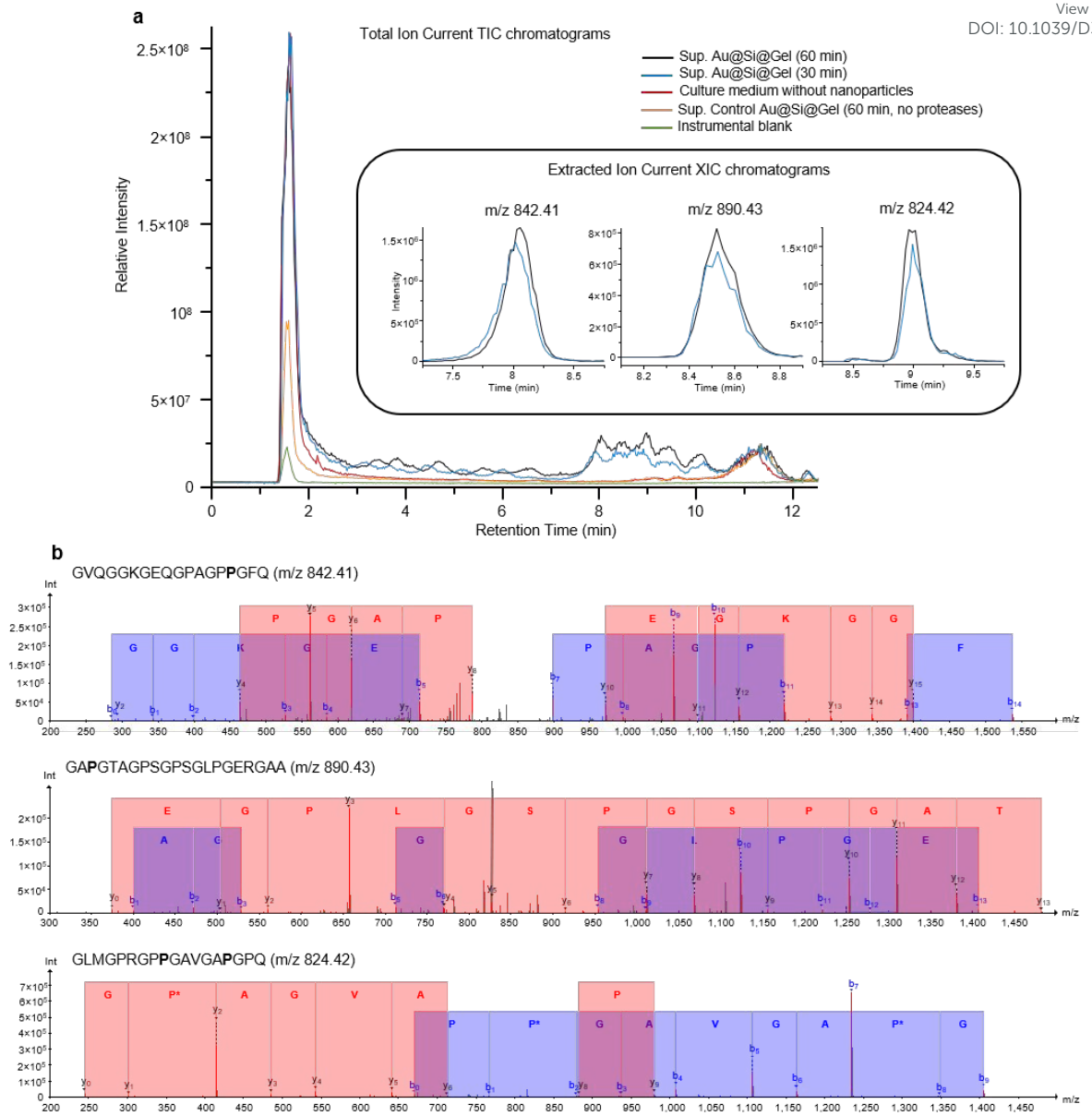

Fig. 6. LC-ESI-MS/MS characterization of the supernatants after incubation with proteases. a, overlay of the total ion current (TIC) chromatograms of the supernatant of Au@Si@Gel nanoparticles for 60 min (black), 30 min (blue), the culture medium without nanoparticles (red) and the supernatant of control Au@Si@Gel nanoparticles (yellow), with three XIC insets showing the intensity change with incubation time. b, MS/MS spectra of the de novo sequenced peptides GVQGGKGEQGPAGPPGFQ (top), GAPGTAGPSGPSGLPGERGAA (middle) and GLMGPRGPPGAVGAPGPQ (bottom), all found in the supernatant of Au@Si@Gel after 60 min of incubation (P = hydroxyproline).

Related to the nature of the proteins found in the positive control of trypsin-digested gelatin, three proteins were found. Collagen type I alpha 2 chain protein with a 22.34% coverage, Collagen type I alpha 1 chain with a 15.09% coverage and Collagen type III alpha 1 chain with a 9.20% coverage (Fig. S5 ESI†). Also, in the supernatant of Au@Si@Gel in culture medium for 60 min, Collagen type I alpha 2 chain protein with a 16.34% coverage and Collagen type I alpha 1 chain with a 2.69% coverage were found, however peptides corresponding to Collagen type III alpha 1 chain were not found in this sample (Fig. S6 ESI†). Furthermore, the absence of these kind of peptides was confirmed in the control Au@Si@Gel supernatant incubated without proteases as well as in the culture medium.

4. Discussion

The mechanisms related to bacteria/nanomaterials interactions in environment especially those focused on the complex processes of microbial biodegradation at nanoscale are poorly studied in literature. However, the nano-scaled biodegradation related mechanisms are of primary importance due to the high bioavailability of nanoparticulated organic matter in ecosystems[23,53]. In the Ocean, phytoplankton releases large amount of dissolved organic matter that is rapidly degraded by heterotrophic bacteria. This process plays a central role in carbon cycling in the Ocean. A large part (30-60%) of this

View Article Online DOI: 10.1039/D3EN00585B

released organic carbon consists of particles with size ranging from 1 nm to 200 nm. Microbial degradation of these nanoparticles generally requires ectoenzymes that hydrolyze macromolecules to smaller compounds that are used by bacteria for growth[18,54].

In addition, the current dissemination in environment of nano-scaled emerging contaminants like nanoplastics or inorganic manufactured nanoparticles constitutes a major issue that can impact ecosystems, especially microbes that are at the lowest trophic level[6,12,20,21]. The ability of nanoparticles to vectorize organic or inorganic contaminants through physical or chemical binding on their surface may interfere with the natural biodegradation processes[20,21,23,55]. Concerning micro- and nanoplastics, the possibility of using microorganisms to biodegrade them is the focus of many studies[15].

However, highlighting by a direct methodology such biodegradation mechanisms occurring on the surface of nanoparticles is challenging and not reported up to now in literature. This implies not only to demonstrate an enzymatic behavior of bacteria toward a given substrate but also an effective accessibility of the enzymes to the substrate at the surface of nanoparticles. We respond to those issues in this work by adopting an approach based on the use of model particles and the implementation of a combination of techniques that allow (i) to probe the chemical composition of the surface of nanoparticles at nanoscale and (ii) to track peptides from the enzymatic degradation process.

Concerning the first point, the model particles have a core-shell architecture to bring several functions in one single unit. Each particle has a single 30 nm gold core that was used as a metal probe to provide a control of the particles concentration. Indeed, SP-ICP-MS allows the quantification in terms of particle concentration through the elemental detection of gold that comes exclusively from the gold core[43]. A silica shell around 65 nm thick was subsequently coated through a sol-gel process on the gold core to provide (i) a platform for the gelatin deposition and (ii) a control of the final size of the particles. For the first point, the deposition of gelatin on the silica shell was carried out through electrostatic interactions due to opposite charges between gelatin and silica. Indeed, the isoelectric points of type A gelatin and silica are 9.5 and 2 respectively leading to positively charged gelatin and negatively charged silica at neutral pH. The TEM images of the Au@Si@Gel attest of the gelatin corona on the silica shell. Concerning the second point, the control of the final size of close to 160 nm is facilitated by the so-called well-known Stöber sol-gel process providing monodispersed silica particles[37].

The study of the biodegradation process was carried out using *A. macleodii* ATCC 27126 as model bacteria. This strain is known to degrade gelatin[26–28] and we demonstrated the presence of proteolytic activity in the culture supernatant. In literature, the production of proteases by *Alteromonas macleodii* has already been demonstrated in studies focused on the topic of dissolved organic matter (DOM). For instance, it has been shown using HPLC and fluorescence imaging that peptide can be completely degraded by *Alteromonas* proteases into individual amino acids. *Alteromonas* use mainly extracellular hydrolysis as decomposition pathway that other bacteria, unable to produce these type of enzymes, may benefit from[56]. In our case, the presence of proteases in the incubation medium was confirmed through a proteolytic azocasein assay[38,39].

Focusing on the gelatin biodegradation, several papers have reported related processes through different methodologies and using different morphology of the gelatin substrates. For instance, the biodegradation of gelatin films by various bacteria and fungi has been studied by indirect impedance, weight loss and dehydrogenase activity[57,58], without in-depth characterizing in detail the gelatin film at nanoscale. More recently, the degradation process on a gelatin-alginate microcapsule by enzymes has been accurately characterized by ^{1}H NMR spectroscopy[59], but the enzymes employed in this study were highly specific to the substrate and did not come from microorganisms. In another study, gelatin nanoparticles coated by red blood cell membranes were studied as an antibiotic delivery system able to release the drug triggered by bacterial exotoxins and using gelatinase-positive bacterial species[60]. In such study, the gelatin is located in the core and no in-depth characterization of the biodegradation process was realized.

In our work, the main objective was to demonstrate a proteolytic behavior of bacteria proteases even when the substrate is only available as a thin coating (less than 10 nm) on nanoparticles. The main question relied on the ability of enzymes to access to the cleavage sites of the substrate in such nanometer scaled confined state, which implies steric constraints that are not encountered in the case of dissolved matter. Moreover, this question remains of a great importance in environment since organic matter adsorbed on natural particles or disseminated nano-scaled contaminants including manufactured particles or nanoplastics alter the bioavailability of substrates in ecosystems. As discussed above, this question cannot be treated without the design of model particles that allow to adjust the physico-chemical parameters for controlling the adsorption behavior of the substrate. But the demonstration of the surface biodegradation process required also a specific methodology based on a combination of analytical techniques able to characterize separately both the supernatant and the surface of particles at nanoscale. To our knowledge, such methodology has never been conducted before.

In a first step, the detailed analysis of the chemical composition of the surface of particles incubated with proteases were realized and has been performed through the characterization of the pellets by ToF-SIMS and XPS. Indeed, such techniques are particularly suitable for the analysis of materials surface at the nanoscale providing chemical information to a depth of 1 nm to 10 nm respectively. For Au@Si@Gel pellets incubated 30 and 60 min, it was possible to detect both characteristic silica peaks (previously detected in the non-incubated Au@Si nanoparticles) and gelatin related peaks, in contrast to reference and control Au@Si@Gel, where the silica peaks were absent or barely detected (Fig. 3, Fig. 5 and Fig. S2 ESI†). Moreover, the silica peaks increased in intensity with incubation time. This was also observed by the XPS quantitative analysis in Fig. 5b supported by the Table S1 in ESI† where

View Article Online
DOI: 10.1039/D3EN00523B

changes in the elemental composition were detected. A clear evolution could be observed in the pellets where the percentage composition in oxygen and silicon increased in direct proportion with incubation time, being higher after 60 minutes of incubation than after 30 minutes, with levels comparable to the Au@Si reference particles. These results are in agreements with the evolution of the amount of carbon and nitrogen elements, which decreases with incubation time.

In a second step, the identification of collagen-related peptides has been made in the supernatants after the incubation with proteases solution by ESI-MS analysis (Fig. 6). In the samples, two proteins were identified, Collagen type I alpha 2 chain (16.34% coverage) and Collagen type I alpha 1 chain (2.69% coverage) from *Sus scrofa*. The same proteins were found in the positive control of trypsin-digested gelatin. Those peptides, not found in control samples (Fig. 6a), were sequenced *de novo* from MS/MS data (Fig. 6b). The full set of sequences is displayed in the Tables S2, S3 and S4 in ESI†. The matching identities of pig collagen peptides in both incubated particles samples and trypsin-digested gelatin control sample confirm the proteolytic behavior against gelatin in the presence of particles. This first step was essential to demonstrate the gelatin biodegradation through the identification of at least 26 peptides in the medium after interactions of Au@Si@Gel nanoparticles with bacteria proteases.

5. Conclusions

Considering the above results, we have demonstrated here for the first time an enzymatic biodegradation process occurring at the surface of nanoparticles. Model core-shell gold/silica/gelatin nanoparticles were synthesized to provide both a control of the substrate adsorption and of the concentration of substrate through the precise quantification by SP-ICP-MS of the number of particles in the solution. Using *Alteromonas macleodii* as model bacteria, we confirm the presence and activity of extracellular enzymes through a proteolytic assay. The accessibility of extracellular proteases to the protein cleavage sites was particularly evidenced by both the identification of peptide amino acid sequences in the medium and the demonstration of organic biodegradation at the surface of the particles. The biodegradation mechanism was characterized through a novel methodology based on the implementation of mass spectrometry and photo-electron spectroscopy highly sensitive techniques able to provide complementary molecular and elemental information at the nanoscale level. LC-ESI-MS/MS was performed to identify in the incubation medium at least 26 pig collagen peptides which were *de novo* sequenced from MS/MS data. XPS and ToF-SIMS/Tandem MS were used to demonstrate the partial gelatin biodegradation at the surface of the particles at the nanoscale level through the characterization of the elemental and molecular composition (depth resolution from 1 nm to 10 nm). The incubation time of particles with proteases had a direct influence on the amount of gelatin degraded. The degradation process led to an increasing exposition of the silica shell with time and concomitantly, a reduction of carbon and nitrogen on the particles surface.

In this study, the control of the physico-chemical parameters has been carried out through the use of model particles and the implementation of reproducible incubation conditions. However, investigations in our group are currently in progress to better understand the effect of the physico-chemical parameters and the type of substrate on the biodegradation process. Especially, the temperature and the pH variation are expected to have a great influence on the extension of the gelatin chains at the particles/water interface which consequently may affect the accessibility of the proteases to the cleavage sites. By varying the type of substrate, the biodegradation behavior might also be affected due to the modulation of the binding process on the particles surface and/or the localization of the cleavage sites.

Author Contributions

Sergio Fernández-Castillo Suárez : conceptualization, methodology, investigation, data curation, writing – original draft. Cécile Courrèges : conceptualization, methodology, investigation, data curation, supervision, validation, funding acquisition, writing – review & editing. Javier Jiménez-Lamana : conceptualization, methodology, investigation, data curation, validation, funding acquisition, writing – review & editing. Simon Godin : conceptualization, methodology, investigation, data curation, validation, funding acquisition, writing – review & editing. Sophie Nolivos : conceptualization, methodology, investigation, validation, writing – review & editing. Régis Grimaud : conceptualization, methodology, investigation, validation, funding acquisition, writing – review & editing. Luisa Ronga : conceptualization, investigation, validation, writing – review & editing. Joanna Szpunar : conceptualization, methodology, investigation, validation, funding acquisition, writing – review & editing. Joachim Allouche : conceptualization, methodology, investigation, data curation, supervision, validation, funding acquisition, writing – review & editing.

Conflicts of interest

There are no conflicts to declare.

Acknowledgements

We would like to acknowledge Arkema (GRL, Lacq, France) for the TEM characterizations. This work was supported by Region Aquitaine, E2S UPPA and ANR funding.

Notes and references

1 M. S. Johal and L. E. Johnson, *Understanding Nanomaterials, Second Edition*, CRC Press, Boca Raton, 2018.
2 C. M. Hussain, Ed., *Handbook of Nanomaterials for Industrial Applications*, Elsevier, 2018.
3 C. Binns, *Introduction to nanoscience and nanotechnology*,

John Wiley & Sons, Inc, Hoboken, NJ, USA, Second edition., 2022.
4 S. Soulé, A.-L. Bulteau, S. Faucher, B. Haye, C. Aimé, J. Allouche, J.-C. Dupin, G. Lespes, T. Coradin and H. Martinez, *Langmuir*, 2016, **32**, 10073–10082.
5 R. Augustine, A. Hasan, R. Primavera, R. J. Wilson, A. S. Thakor and B. D. Kevadiya, *Mater. Today Commun.*, 2020, **25**, 101692.
6 F. Ameen, K. Alsamhary, J. A. Alabdullatif and S. ALNadhari, *Ecotoxicol. Environ. Saf.*, 2021, **213**, 112027.
7 A. Nel, T. Xia, L. Mädler and N. Li, *Science*, 2006, **311**, 622–627.
8 B. Fadeel, A. Pietroiusti and A. A. Shvedova, Eds., *Adverse effects of engineered nanomaterials: exposure, toxicology, and impact on human health*, Elsevier/Academic Press, London, Second edition., 2017.
9 R. Van Der Meel, E. Sulheim, Y. Shi, F. Kiessling, W. J. M. Mulder and T. Lammers, *Nat. Nanotechnol.*, 2019, **14**, 1007–1017.
10 C. Ganzleben and S. Foss Hansen, *Environmental Exposure to Nanomaterials Data Scoping Study*, 2012.
11 A. E. Nel, L. Mädler, D. Velegol, T. Xia, E. M. V. Hoek, P. Somasundaran, F. Klaessig, V. Castranova and M. Thompson, *Nat. Mater.*, 2009, **8**, 543–557.
12 K. Ikuma, A. W. Decho and B. L. T. Lau, *Front. Microbiol.*, , DOI:10.3389/fmicb.2015.00591.
13 S. D. Richardson and S. Y. Kimura, *Anal. Chem.*, 2020, **92**, 473–505.
14 M. Taheran, M. Naghdi, S. K. Brar, M. Verma and R. Y. Surampalli, *Environ. Nanotechnol. Monit. Manag.*, 2018, **10**, 122–126.
15 M. Mofijur, S. F. Ahmed, S. M. A. Rahman, Sk. Y. Arafat Siddiki, A. B. M. S. Islam, M. Shahabuddin, H. C. Ong, T. M. I. Mahlia, F. Djavanroodi and P. L. Show, *Environ. Res.*, 2021, **195**, 110857.
16 M. P. Shah, Ed., *Microbial Bioremediation & Biodegradation*, Springer Singapore, Singapore, 2020.
17 H. Hemeg, *Int. J. Nanomedicine*, 2017, **12**, 8211–8225.
18 R. Benner and R. M. W. Amon, *Annu. Rev. Mar. Sci.*, 2015, **7**, 185–205.
19 H. M. N. Iqbal, M. Bilal, T. A. Nguyen and G. Yasin, Eds., *Biodegradation and Biodeterioration At the Nanoscale*, Elsevier, 2022.
20 M. C. Rillig, E. Leifheit and J. Lehmann, *PLOS Biol.*, 2021, **19**, e3001130.
21 M. Shen, S. Liu, T. Hu, K. Zheng, Y. Wang and H. Long, *J. Environ. Manage.*, 2023, **334**, 117529.
22 S. Iravani, *Int. Sch. Res. Not.*, 2014, **2014**, 1–18.
23 M. Mansor and J. Xu, *Environ. Microbiol.*, 2020, **22**, 3633–3649.
24 S. Yu, J. Liu, Y. Yin and M. Shen, *J. Environ. Sci.*, 2018, **63**, 198–217.
25 C. Courrèges, M. Bonnecaze, D. Flahaut, S. Nolivos, R. Grimaud and J. Allouche, *Chem. Commun.*, 2021, **57**, 5446–5449.
26 L. Baumann, P. Baumann, M. Mandel and R. D. Allen, *J. Bacteriol.*, 1972, **110**, 402–429.
27 V. V. Mikhailov, L. A. Romanenko and E. P. Ivanova, in *The Prokaryotes*, eds. M. Dworkin, S. Falkow, E. Rosenberg, K.-H. Schleifer and E. Stackebrandt, Springer New York, New York, NY, 2006, pp. 597–645.
28 M. López-Pérez and F. Rodriguez-Valera, in *The Prokaryotes*, eds. E. Rosenberg, E. F. DeLong, S. Lory, E. Stackebrandt and F. Thompson, Springer Berlin Heidelberg, Berlin, Heidelberg, 2014, pp. 69–92.
29 A. Gonzaga, M. López-Pérez, A.-B. Martin-Cuadrado, R. Ghai and F. Rodriguez-Valera, *J. Bacteriol.*, 2012, **194**, 6998–6998.
30 M. López-Pérez, A. Gonzaga, A.-B. Martin-Cuadrado, O. Onyshchenko, A. Ghavidel, R. Ghai and F. Rodriguez-Valera, *Sci. Rep.*, 2012, **2**, 696.
31 B. E. Pedler, L. I. Aluwihare and F. Azam, *Proc. Natl. Acad. Sci.*, 2014, **111**, 7202–7207.
32 H. Koch, A. Dürwald, T. Schweder, B. Noriega-Ortega, S. Vidal-Melgosa, J.-H. Hehemann, T. Dittmar, H. M. Freese, D. Becher, M. Simon and M. Wietz, *ISME J.*, 2019, **13**, 92–103.
33 L. E. Manck, J. L. Espinoza, C. L. Dupont and K. A. Barbeau, *mSystems*, 2020, **5**, e00070-20.
34 L. E. Manck, J. Park, B. J. Tully, A. M. Poire, R. M. Bundy, C. L. Dupont and K. A. Barbeau, *ISME J.*, 2022, **16**, 358–369.
35 E. Ivars-Martinez, A.-B. Martin-Cuadrado, G. D'Auria, A. Mira, S. Ferriera, J. Johnson, R. Friedman and F. Rodriguez-Valera, *ISME J.*, 2008, **2**, 1194–1212.
36 J. Dong, P. L. Carpinone, G. Pyrgiotakis, P. Demokritou and B. M. Moudgil, *KONA Powder Part. J.*, 2020, **37**, 224–232.
37 W. Stöber, A. Fink and E. Bohn, *J. Colloid Interface Sci.*, 1968, **26**, 62–69.
38 J. Charney and R. M. Tomarelli, *J. Biol. Chem.*, 1947, **171**, 501–505.
39 D. F. Coêlho, T. P. Saturnino, F. F. Fernandes, P. G. Mazzola, E. Silveira and E. B. Tambourgi, *BioMed Res. Int.*, 2016, **2016**, 1–6.
40 T. Muth, L. Weilnböck, E. Rapp, C. G. Huber, L. Martens, M. Vaudel and H. Barsnes, *J. Proteome Res.*, 2014, **13**, 1143–1146.
41 The UniProt Consortium, A. Bateman, M.-J. Martin, S. Orchard, M. Magrane, S. Ahmad, E. Alpi, E. H. Bowler-Barnett, R. Britto, H. Bye-A-Jee, A. Cukura, P. Denny, T. Dogan, T. Ebenezer, J. Fan, P. Garmiri, L. J. da Costa Gonzales, E. Hatton-Ellis, A. Hussein, A. Ignatchenko, G. Insana, R. Ishtiaq, V. Joshi, D. Jyothi, S. Kandasaamy, A. Lock, A. Luciani, M. Lugaric, J. Luo, Y. Lussi, A. MacDougall, F. Madeira, M. Mahmoudy, A. Mishra, K. Moulang, A. Nightingale, S. Pundir, G. Qi, S. Raj, P. Raposo, D. L. Rice, R. Saidi, R. Santos, E. Speretta, J. Stephenson, P. Totoo, E. Turner, N. Tyagi, P. Vasudev, K. Warner, X. Watkins, R. Zaru, H. Zellner, A. J. Bridge, L. Aimo, G. Argoud-Puy, A. H. Auchincloss, K. B. Axelsen, P. Bansal, D. Baratin, T. M. Batista Neto, M.-C. Blatter, J. T. Bolleman, E. Boutet, L. Breuza, B. C. Gil, C. Casals-Casas, K. C. Echioukh, E. Coudert, B. Cuche, E. de Castro, A. Estreicher, M. L. Famiglietti, M. Feuermann, E. Gasteiger, P. Gaudet, S. Gehant, V. Gerritsen, A. Gos, N. Gruaz, C. Hulo, N. Hyka-Nouspikel, F. Jungo, A. Kerhornou, P. Le Mercier, D. Lieberherr, P. Masson, A. Morgat, V. Muthukrishnan, S. Paesano, I. Pedruzzi, S. Pilbout, L. Pourcel, S. Poux, M. Pozzato, M. Pruess, N. Redaschi, C. Rivoire, C. J. A. Sigrist, K. Sonesson, S. Sundaram, C. H. Wu, C. N. Arighi, L. Arminski, C. Chen, Y. Chen, H. Huang, K. Laiho, P. McGarvey, D. A. Natale, K. Ross, C. R. Vinayaka, Q. Wang, Y. Wang and J. Zhang, *Nucleic Acids Res.*, 2023, **51**, D523–D531.
42 R. T. Fellers, J. B. Greer, B. P. Early, X. Yu, R. D. LeDuc, N. L. Kelleher and P. M. Thomas, *PROTEOMICS*, 2015, **15**, 1235–1238.
43 F. Laborda, E. Bolea and J. Jiménez-Lamana, *Anal. Chem.*, 2014, **86**, 2270–2278.
44 J. B. Ledeuil, A. Uhart, S. Soulé, J. Allouche, J. C. Dupin and H. Martinez, *Nanoscale*, 2014, **6**, 11130–11140.
45 S. Soulé, J. Allouche, J.-C. Dupin and H. Martinez, *Microporous Mesoporous Mater.*, 2013, **171**, 72–77.
46 J. Allouche, S. Soulé, J.-C. Dupin, S. Masse, T. Coradin and H. Martinez, *RSC Adv*, 2014, **4**, 63234–63237.
47 J. Allouche, C. Chanéac, R. Brayner, M. Boissière and T. Coradin, *Nanomaterials*, 2014, **4**, 612–627.
48 G. Zhang, T. Liu, Q. Wang, L. Chen, J. Lei, J. Luo, G. Ma and Z. Su, *Food Hydrocoll.*, 2009, **23**, 2001–2007.
49 M. T. Yilmaz, Z. Kesmen, B. Baykal, O. Sagdic, O. Kulen, O. Kacar, H. Yetim and A. T. Baykal, *Food Chem.*, 2013, **141**, 2450–2458.
50 C. T. Yang, D. Ghosh and F. Beaudry, *Food Addit. Contam. Part A*, 2018, **35**, 599–608.

View Article Online
DOI: 10.1039/D3EN00523B

51 A. J. Kleinnijenhuis, F. L. van Holthoon and G. Herregods, *Food Chem.*, 2018, **243**, 461–467.
52 M. Valletta, S. Ragucci, N. Landi, A. Di Maro, P. V. Pedone, R. Russo and A. Chambery, *Food Chem.*, 2021, **365**, 130456.
53 P. Sivadon, C. Barnier, L. Urios and R. Grimaud, *Environ. Microbiol. Rep.*, 2019, 1758-2229.12785.
54 C. Arnosti, *Annu. Rev. Mar. Sci.*, 2011, **3**, 401–425.
55 A. Aynard, C. Courrèges, J. Jiménez-Lamana, A. Raad, C. Miqueu, B. Grassl and S. Reynaud, *Environ. Pollut.*, 2023, **323**, 121229.
56 S. Liu and Z. Liu, *Sci. Rep.*, 2020, **10**, 464.
57 P. Dalev, E. Staromanova, D. Dalev, R. D. Patil, J. E. Mark, E. Vassileva and S. Fakirov, *Biotechnol. Biotechnol. Equip.*, 2001, **15**, 116–123.
58 C. Abrusci, D. Marquina, A. Del Amo and F. Catalina, *Int. Biodeterior. Biodegrad.*, 2007, **60**, 137–143.
59 U. T. Do, J. Kim, Q. S. Luu, Q. T. Nguyen, T. Jang, Y. Park, H. Shin, N. Whiting, D.-K. Kang, J.-S. Kwon and Y. Lee, *Carbohydr. Polym.*, 2023, **304**, 120490.
60 L.-L. Li, J.-H. Xu, G.-B. Qi, X. Zhao, F. Yu and H. Wang, *ACS Nano*, 2014, **8**, 4975.